TU Delft

Delft University of Technology

Document Version
Final published version

Licence
Dutch Copyright Act (Article 25fa)

Citation (APA)
Chen, Y., Li, Y., Xue, Y., Li, Z., Zeng, Y., Chen, X., Zhao, Y., & Zhang, Y. (2026). Activation of retarded seawater-mixed cementitious materials for 2K 3D concrete printing. *Construction and Building Materials*, *530*, Article 146645. https://doi.org/10.1016/j.conbuildmat.2026.146645

Important note
To cite this publication, please use the final published version (if applicable).
Please check the document version above.

Copyright
In case the licence states “Dutch Copyright Act (Article 25fa)”, this publication was made available Green Open Access via the TU Delft Institutional Repository pursuant to Dutch Copyright Act (Article 25fa, the Taverne amendment). This provision does not affect copyright ownership.
Unless copyright is transferred by contract or statute, it remains with the copyright holder.

Sharing and reuse
Other than for strictly personal use, it is not permitted to download, forward or distribute the text or part of it, without the consent of the author(s) and/or copyright holder(s), unless the work is under an open content license such as Creative Commons.

Takedown policy
Please contact us and provide details if you believe this document breaches copyrights.
We will remove access to the work immediately and investigate your claim.

This work is downloaded from Delft University of Technology.

Construction and Building Materials 530 (2026) 146645

Contents lists available at ScienceDirect

Construction and Building Materials

journal homepage: www.elsevier.com/locate/conbuildmat

Activation of retarded seawater-mixed cementitious materials for 2K 3D concrete printing

Yu Chen [a,b,*], Yao Li [a], Yiqun Xue [a], Zhipeng Li [a], Yu Zeng [c], Xusheng Chen [a], Yilin Zhao [a], Yamei Zhang [a,b,*]

[a] State Key Laboratory of Engineering Materials for Major Infrastructure, School of Materials Science and Engineering, Southeast University, Nanjing 211189, China
[b] Nanjing Institute for Intelligent Additive Manufacturing, Nanjing 211800, China
[c] Microlab, Faculty of Civil Engineering and Geosciences, Delft University of Technology, Delft, the Netherlands

ARTICLE INFO

Keywords:
3D concrete printing
Seawater-mixed concrete
Rheology
Structural build-up
Early-age hydration

ABSTRACT

Seawater-mixed concrete for 3D printing offers a promising solution for marine infrastructure construction in coastal and island regions facing shortages of freshwater and labor. However, the high chloride concentration in seawater accelerates the initial setting of concrete, thereby hindering pumping and extrusion in one-component (1 K) printing. The two-component (2 K) printing approach, which combines retarded cementitious mixtures with aluminate-based accelerators, enables set-on-demand behavior and provides a potential solution for seawater-based printing. Nevertheless, the early-age behavior of seawater-mixed cementitious materials incorporating aluminate-based accelerators, such as aluminum sulfate (A$) and calcium aluminate cement with anhydrite (CAC-C$), remains largely unexplored, particularly regarding their interactions with seawater ions and Portland cement. This study systematically investigates the structural build-up and early-age hydration of seawater-mixed cementitious materials incorporating A$- and CAC-C$-based acceleration slurries. Structural build-up was quantified using constant shear rate rheometry, while water state evolution, hydration kinetics, and phase assemblages were characterized using low-field ^{1}H NMR, isothermal calorimetry, thermogravimetric analysis, and X-ray diffraction. The results demonstrate that ettringite (AFt) precipitation governs structural build-up in both systems due to its high water-binding capacity and voluminous needle-like morphology. Seawater significantly enhances AFt formation in the A$-based system, leading to rapid stiffening but a narrowed printability window. In contrast, seawater initially suppresses AFt formation in the CAC-C$ system due to delayed sulfate dissolution and the preferential formation of Friedel's salt; this effect is transient, and AFt formation resumes at later ages. Consequently, the CAC-C$ system exhibits superior robustness and greater suitability for seawater-mixed concrete 2 K printing.

1. Introduction

Many coastal and island regions worldwide face severe freshwater shortages, posing significant constraints on concrete infrastructure development. Seawater has therefore been proposed as an alternative mixing water for concrete production [1,2]. However, its high chloride content can cause severe corrosion of steel reinforcement, necessitating the use of corrosion-resistant alternatives such as fiber-reinforced polymer (FRP) reinforcement [3]. In addition to durability concerns, seawater significantly alters the fresh-state behavior of cementitious materials. The major dissolved ions in seawater, including Cl^-, Na^+, Ca^{2+}, and Mg^{2+}, have been shown to accelerate workability loss, initial setting, and structural build-up [4–6]. While such acceleration is detrimental to conventional casting processes, it may offer advantages for additive manufacturing that require rapid structural development.

Extrusion-based 3D concrete printing (3DCP) has emerged as a promising digital construction technology due to its ability to fabricate structures without formwork, thereby reducing labor demand, material consumption, and construction time while enabling greater design flexibility [7–12]. These advantages make 3DCP particularly attractive for infrastructure construction in coastal and island regions, where labor shortages and logistical constraints present significant challenges.

* Corresponding authors at: State Key Laboratory of Engineering Materials for Major Infrastructure, School of Materials Science and Engineering, Southeast University, Nanjing 211189, China.
E-mail addresses: y_chen@seu.edu.cn (Y. Chen), ymzhang@seu.edu.cn (Y. Zhang).

https://doi.org/10.1016/j.conbuildmat.2026.146645
Received 18 February 2026; Received in revised form 4 May 2026; Accepted 7 May 2026
Available online 13 May 2026
0950-0618/© 2026 Elsevier Ltd. All rights are reserved, including those for text and data mining, AI training, and similar technologies.

Table 1
Oxide compositions of PC, CAC, quartz powder and A$.

XRF [wt%]	PC	CAC	Quartz powder	A$
CaO	61.58	34.37	0.02	0.06
SiO_2	16.14	7.55	98.52	0.03
Al_2O_3	3.73	47.89	0.15	13.56
Fe_2O_3	2.31	1.7	0.02	0.08
MgO	3.36	0.7	0.01	0.1
Na_2O	0.29	0.09	0.01	0.07
K_2O	0.89	0.31	0.02	0.01
SO_3	3.44	0.56	< 0.01	37.87
Others	5.42	2.48	1	0.02
LOI (950 °C)	2.84	4.35	0.25	48.2

However, the absence of formwork imposes stringent and often conflicting rheological requirements on printable cementitious materials: the mixture must remain highly flowable during pumping and extrusion while rapidly developing sufficient stiffness after deposition to support subsequent layers [13–15]

Two main strategies have been developed for 3DCP, i.e., one-component (1 K) and two-component (2 K) printing [16]. In the 1 K approach, all constituents are premixed prior to pumping, and buildability of fresh mixture is primarily achieved through thixotropic structural recovery [17–20]. However, this approach is inherently limited by the trade-off between pumpability and buildability, particularly in large-scale applications requiring long pumping distances and extended open times [21,22]. These challenges are further exacerbated in seawater-mixed cementitious materials, where the presence of dissolved ions accelerates stiffness evolution [22], reducing pumpability and printability windows. The 2 K printing approach, also referred to as set-on-demand printing, provides an effective solution to this limitation by enabling independent control of pumpability and structural build-up [16,23,24]. In this method, a highly flowable, retarded cementitious mixture is first transported to the printhead, where it is inline mixed with an accelerator immediately prior to extrusion [25,26]. This strategy allows hydration to remain temporarily suppressed during pumping and subsequently reactivated at the nozzle to induce rapid stiffening and structural build-up [14,15,27–29]. Such controlled activation is particularly advantageous for seawater-mixed systems, enabling the formulation of pumpable “dormant” mixtures that can be rapidly “activated” before deposition.

Accelerators used in 2 K printing typically promote the formation of either calcium silicate hydrate (C-S-H) or ettringite (AFt) [12]. While calcium salts or C-S-H seeding can accelerate silicate hydration [15,28,30], AFt-based acceleration is generally more effective in inducing rapid structural build-up due to its ability to form an interlocking crystalline network [12,29,31]. Consequently, aluminum-rich accelerators such as aluminate-sulfate admixtures, calcium aluminate cement, and calcium sulfoaluminate are widely employed [12,29,30]. However, the introduction of additional aluminates alters the chemical equilibrium of the system and may inhibit C_3S hydration when present in high concentrations, potentially compromising long-term strength development [31,32]. In seawater-mixed systems, the presence of abundant ions, including Cl^-, Na^+, Ca^{2+}, SO_4^{2+}, and Mg^{2+}, further complicates hydration and structuration processes. These ions can influence both aluminate and silicate reactions through competitive precipitation, ion adsorption, and phase transformation. For example, seawater has been reported to retard the hydration of cubic C_3A through the coexistence Ca^{2+} and SO_4^{2-} adsorption and the formation of Friedel’s salt, thereby modifying aluminate availability and dissolution kinetics [33]. At the same time, chloride and calcium ions may accelerate C_3S hydration [5,22]. These competing effects suggest that seawater ions may significantly influence the efficiency of AFt-based acceleration and the resulting structural build-up behavior. However, the coupled interactions among seawater ions, Portland cement phases, and aluminate-based accelerators, and their combined effects on rheological properties and hydration, remain poorly understood.

While earlier studies [24,30,34,35] have investigated accelerator-controlled structuration and early hydration, most have focused on freshwater systems or on the general effects of accelerators, without systematically considering the role of seawater. In contrast, the present study specifically examines the combined influence of seawater ions and aluminate-based accelerators within a 2 K activation framework. By quantifying structural build-up and early-age hydration under these conditions, this work provides new insights into how seawater chemistry interacts with reactions induced by aluminate-based accelerators, thereby offering guidance for the design of seawater-mixed cementitious materials for 2 K 3D concrete printing.

Therefore, the objective of this study is to elucidate the interactions among seawater ions, Portland cement, and aluminate-based accelerators, including aluminum sulfate and calcium aluminate cement with anhydrite, and their effects on structural build-up and early-age hydration. Structural build-up was quantified using constant shear rate rheometry, while water state evolution was monitored using low-field

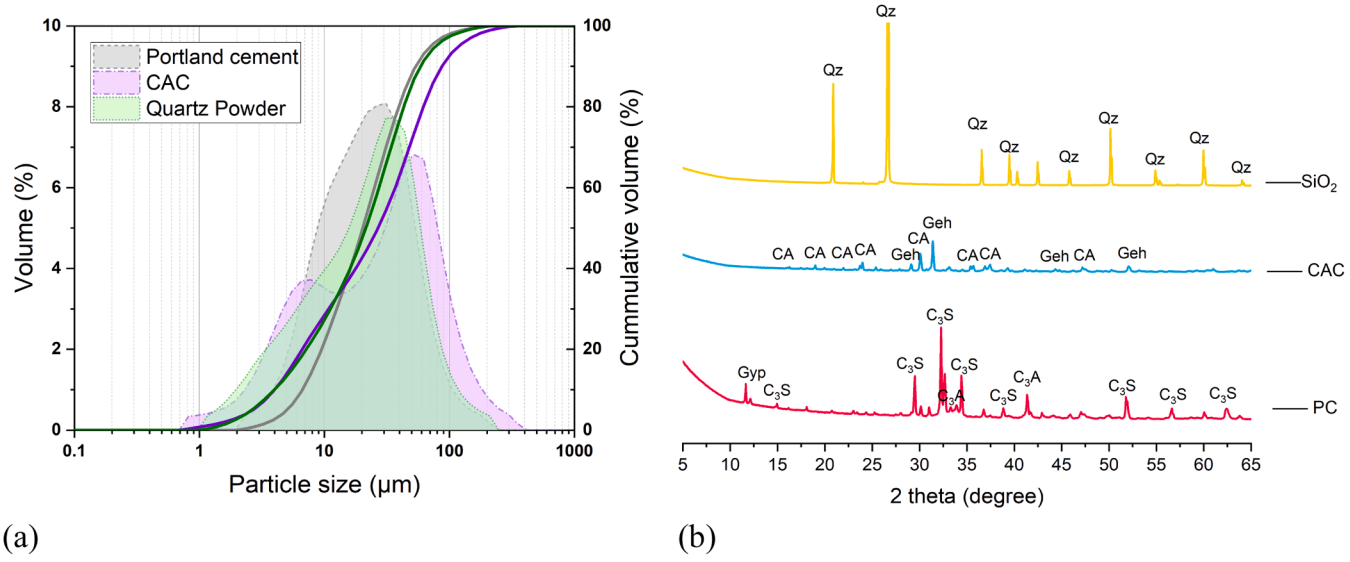


Fig. 1. (a) Particle size distribution of PC, CAC and quartz powder determined by laser diffractometry; (b) XRD patterns of PC, CAC and quartz powder. Qz- quartz; CA- calcium aluminate; Geh- gehlenite; C_3S- alite; C_3A- aluminite; Gyp- gypsum.

Table 2
Physical characteristics of PC, CAC and quartz powder.

	D10 (μm)	D50 (μm)	D90 (μm)	BET specific surface area (m^2/g)	Density (g/cm^3)
PC	6.68	20.24	53.72	0.62	3.15
CAC	4.00	26.90	87.15	0.43	3.00
Quartz powder	3.99	21.49	58.60	0.56	2.65

Table 3
The salt composition of seawater used in this study.

Salts	NaCl	$MgCl_2{\cdot}6\,H_2O$	Na_2SO_4	$CaCl_2$	KCl
Seawater (g/L)	24.35	10.21	3.97	1.45	0.61

^{1}H nuclear magnetic resonance (NMR). Hydration kinetics and phase assemblages were characterized using isothermal calorimetry, thermogravimetric analysis (TGA), and X-ray diffraction (XRD). Finally, the underlying mechanisms governing rheological and hydration evolution in seawater-mixed cementitious materials with aluminate-based accelerators were discussed.

2. Materials and methods

2.1. Raw materials and mix designs

In this study, P·II 42.5 grade Portland cement (PC) was used as the binding material. Aluminate sulfate octadecahydrate (A$) and calcium aluminate cement (CAC) with anhydrite (C$) were employed as the main additives in the acceleration slurry. Fine quartz powder was used as an inert filler. The main chemical compositions of these materials are presented in Table 1. The particle size distributions and crystalline phases of PC, CAC and quartz powder are shown in Fig. 1. Table 2 summarizes the D50 of particle size, density and the BET specific surface areas that were quantified using nitrogen adsorption of PC, CAC and quartz powder. The seawater is acquired from Yellow Sea of China area. The ion composition of seawater was analyzed by Inductively Coupled Plasma-Mass Spectrometry (ICP-MS) and Ion Chromatograph (IC), see Table A1 (Appendix). Based on the main ion composition of seawater, artificial seawater was made and used as the mixing water, as shown in Table 3.

Since two types of accelerators were used in this study, two corresponding series of mix designs were developed, as shown in Tables 4 and 5. Each mix design consists of two components: cementitious material (Part A) and acceleration slurry (Part B). The mass ratio between the Part A and Part B was approximately 2.48:1, based on preliminary tests. It is noteworthy that the composition of the Part A was kept identical across both series. The water-to-cement ratio (W/C) was fixed at 0.3. To enhance the flowability of the Part A, 0.12% (by mass of PC) of a polycarboxylate ether-based superplasticizer (SP) was added. Additionally, 0.03% (by mass of PC) of sucrose was incorporated to mitigate flow loss in the Part A within the first 3 h. The initial and final setting times of the Part A were 252 min and 439 min, respectively.

Both acceleration slurries included quartz powder, in addition to their respective accelerating agents and mixing water. As noted in Refs. [22,36], directly injecting an acceleration solution into the cementitious material can significantly lower the solid-to-liquid ratio, thereby reducing the yield stress and impairing buildability. To overcome this limitation, quartz powder was added as an inert filler to the acceleration slurries. This approach not only improved the rheological performance but also ensured that the solid content remained consistent between the two slurry systems.

For the A$-based acceleration slurry, the formulation consisted of 5–7% A$, 30.5–32.5% quartz powder, and 15% mixing water, all calculated based on the mass of PC. The CAC-C$-based acceleration slurry was designed with a comparable solid content (approximately 37.5% of the PC mass) and a similar mixing water content (15% of the PC mass). Following the recommendation in [12,30], the mass ratio of CAC to C$ was maintained at 2:1. To counteract the rapid setting caused by the hydraulic reactivity of CAC-C$, 0.15% sodium gluconate (SG), based on the mass of CAC, was added to delay the setting and improve workability. The initial setting time of CAC-C$-based acceleration slurry in this study is longer than 200 min. Note that the content of A$ and CAC was determined based on preliminary tests. For most mixtures, seawater (SW) was used as the mixing water for both the Part A and Part B. However, for the reference mixtures, namely 6%A$-FW and 15% CAC-FW, deionized water was used instead in both components. Note that the dosage ranges of A$ and CAC in Part B were determined based on preliminary tests.

Fig. 2 illustrates the workflow of the 2 K 3DCP. As shown, the fresh mixtures of Part A and Part B are prepared separately. After being conveyed to the printhead, the two mixtures are inline-mixed to form the final mixture prior to layer extrusion. In this study, all mixtures were

Table 4
Mix designs of seawater-mixed cementitious materials incorporating with A$-based acceleration slurry (wt% of the PC).

	Cementitious material (Part A)				Acceleration slurry (Part B)		
	PC	Mixing water	SP	Sucrose	A$	Mixing water	Quartz powder
5%A$-SW	100	30	0.12	0.03	5	15	32.5
6%A$-SW	100	30	0.12	0.03	6	15	31.5
7%A$-SW	100	30	0.12	0.03	7	15	30.5
6%A$-FW	100	30	0.12	0.03	6	15	31.5

*Mixture with "SW": mixing water is seawater; Mixture with "FW": mixing water is deionized water. PC, SP and A$ denote Portland cement, superplasticizer and aluminate sulfate octadecahydrate.

Table 5
Mix designs of seawater-mixed cementitious materials incorporating with CAC-C$-based acceleration slurry (wt% of the PC).

	Cementitious material (Part A)				Acceleration slurry (Part B)				
	PC	Mixing water	SP	Sucrose	CAC	Anhydrite	SG	Mixing water	Quartz Powder
10%CAC-SW	100	30	0.12	0.03	10	5	0.015	15	22.5
15%CAC-SW	100	30	0.12	0.03	15	7.5	0.0225	15	15
20%CAC-SW	100	30	0.12	0.03	20	10	0.03	15	7.5
15%CAC-FW	100	30	0.12	0.03	15	7.5	0.0225	15	15

*Mixture with "SW": mixing water is seawater; Mixture with "FW": mixing water is deionized water. PC, SP, CAC and SG denote Portland cement, superplasticizer, calcium aluminate cement and sodium gluconate.

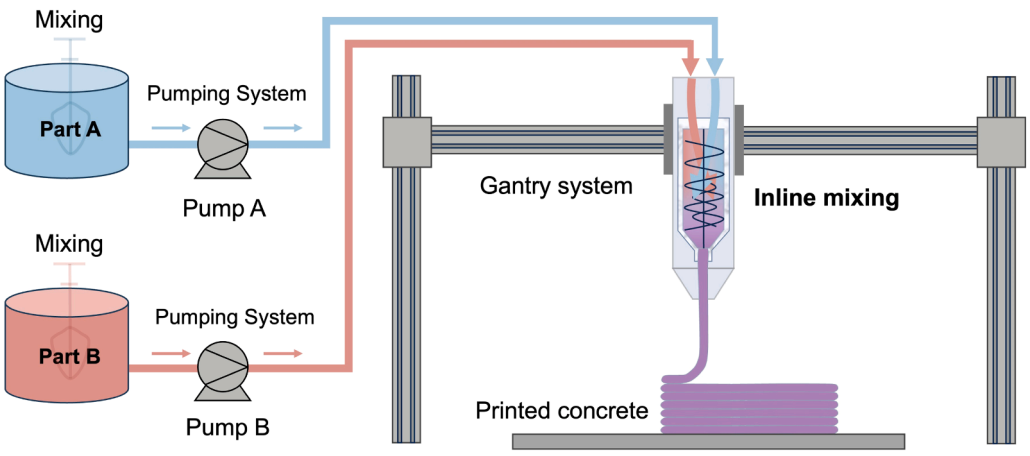


Fig. 2. Schematic illustration of the 2 K 3DCP configuration.

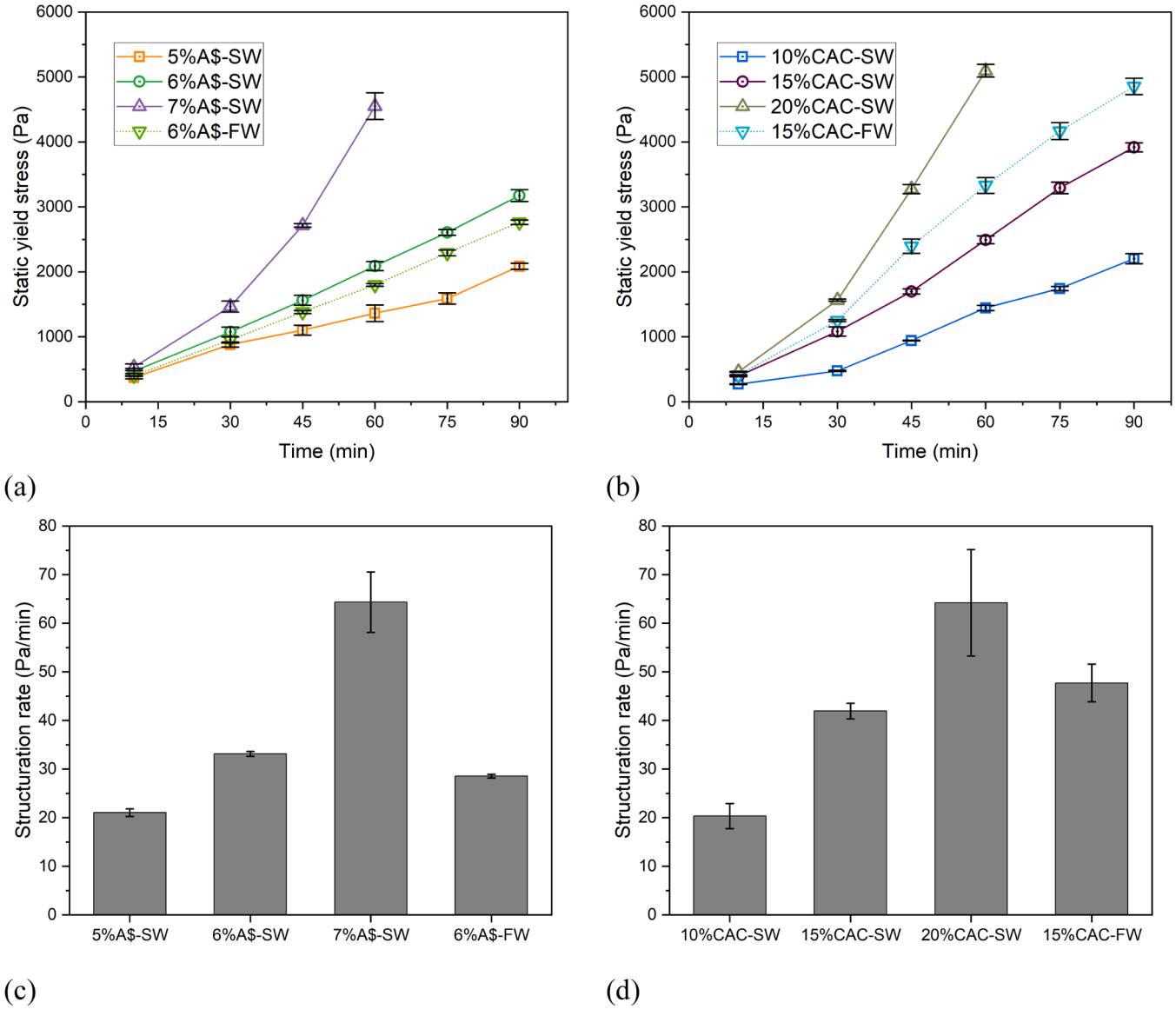


Fig. 3. (a) Static yield stress of cementitious material incorporating with A$-based acceleration slurry; (b) Static yield stress of cementitious material incorporating with CAC-C$-based acceleration slurry; (c) Structuration rate of cementitious material incorporating with A$-based acceleration slurry; (d) Structuration rate of cementitious material incorporating with CAC-C$-based acceleration slurry.

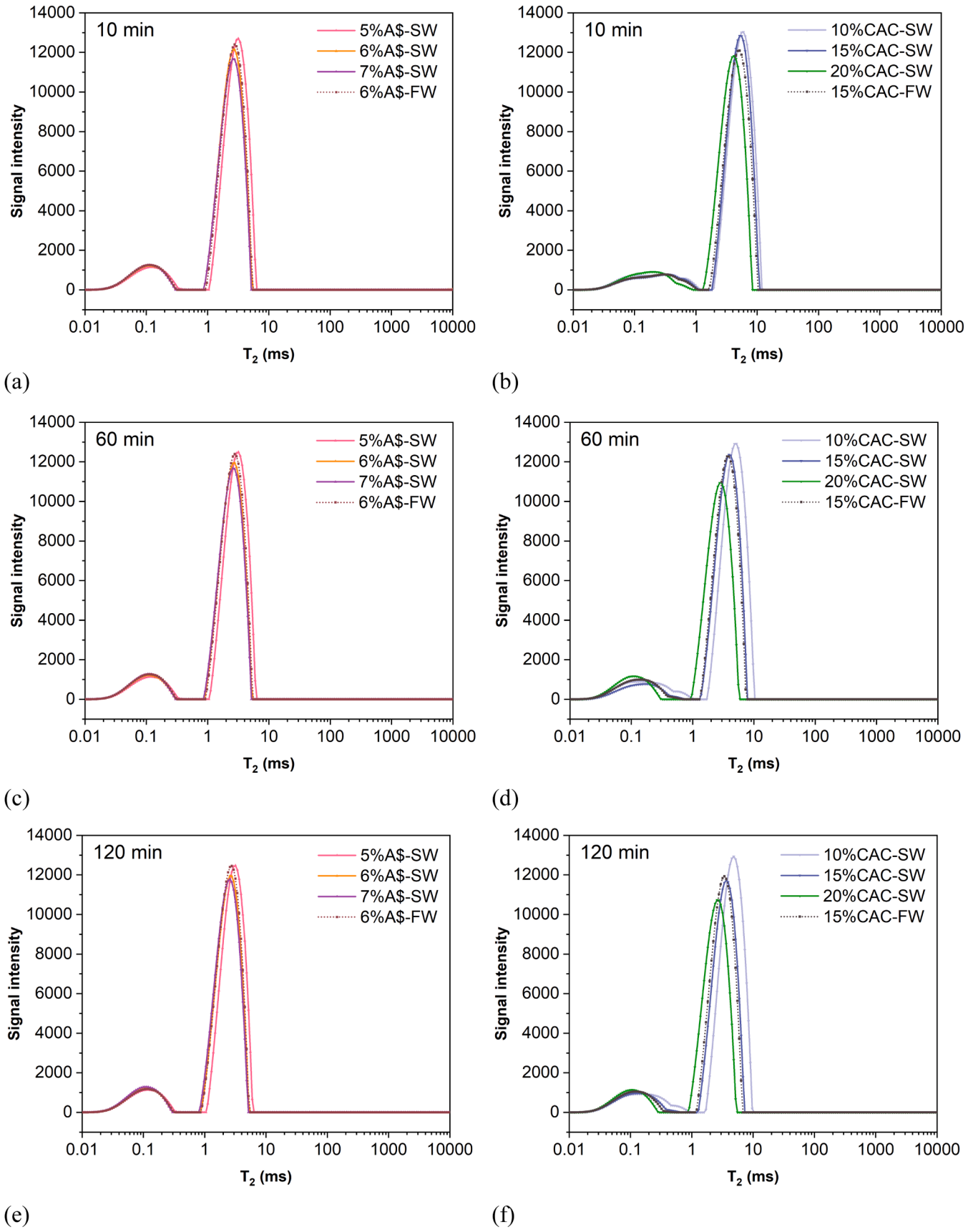


Fig. 4. Comparison of low-field ^{1}H NMR (T_2) spectrums at different ages: (a) 10 min, (c) 60 min and (e) 120 min of cementitious material incorporating with A $-based acceleration slurry; (b) 10 min, (d) 60 min and (f) 120 min of cementitious material incorporating with CAC-C$-based acceleration slurry.

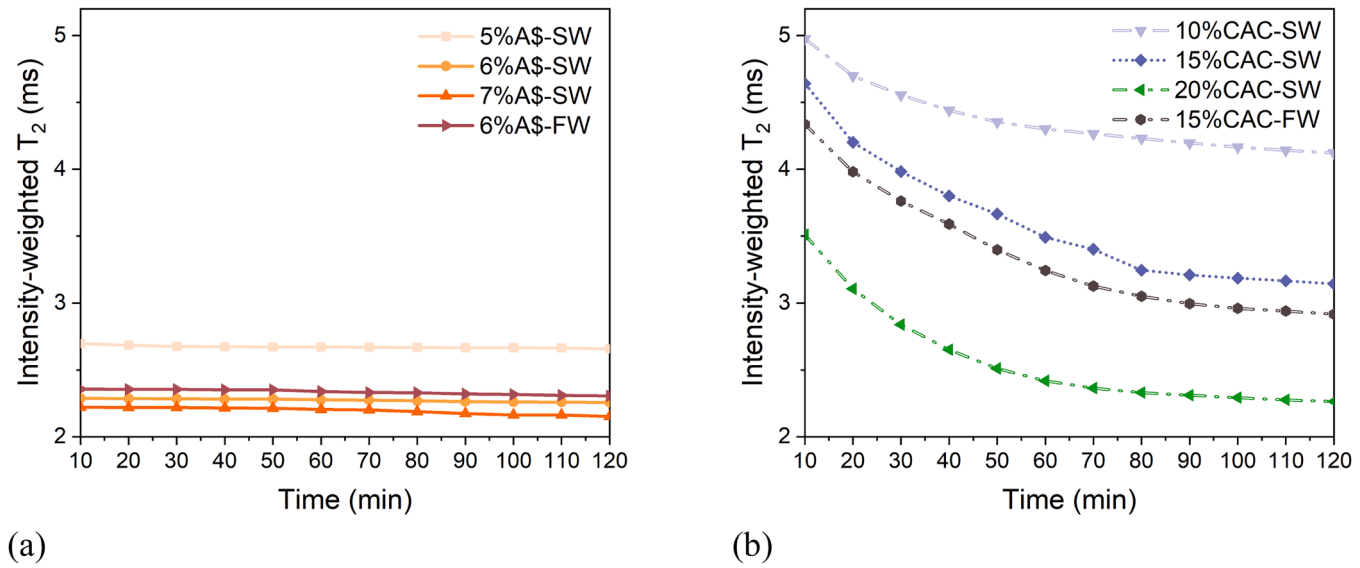


Fig. 5. The T_2 weighted mean value ($\overline{T_2}$) evolution of different studied mixtures within the first 2 h: (a) Cementitious material incorporating with A$-based acceleration slurry; (b) Cementitious material incorporating with CAC-C$-based acceleration slurry.

prepared following the same mixing protocol using a planetary mixer equipped with a flat beater. First, the dry components of the Part B were dry-mixed for 30 s. Then, mixing water was added, and the mixture was stirred at 140 rpm for 60 s to obtain a homogeneous acceleration slurry. Simultaneously, PC and sucrose were premixed for 30 s, followed by the addition of mixing water and stirring at 285 rpm for 90 s to produce the Part A. After that, the prepared Part B was rapidly added into the Part A, and the final mixture was subjected to high-shear mixing at 400 rpm for 30 s. Time zero (t = 0 min) is defined as the moment when Parts A and B are fully mixed.

2.2. Experimental tests

2.2.1. Static yield stress measurement and oscillatory rheological test

A constant shear rate (CSR) test was employed to determine the static yield stress of the proposed mixtures at material ages of 10, 30, 45, 60, 75, and 90 min. All measurements were conducted using a Brookfield RST-SST rheometer equipped with a vane-in-cup setup. For each mixture, a pre-shear step was applied at a constant shear rate of 200 s^{-1} for 1 min at a material age of 8 min, followed by a resting period of 1 min prior to the CSR test. During the CSR test, a constant shear rate of 0.1 s^{-1} was applied for 1 min. After each CSR measurement, the material was allowed to rest until the next testing session. The peak stress value obtained from the curve was taken as the static yield stress at the corresponding material age. In this study, the static yield stress was operationally defined as the peak stress recorded during the CSR test, and should therefore be regarded as a test-dependent measure rather than an intrinsic material constant.

The small-amplitude oscillatory shear (SAOS) test, also referred to as a time sweep test, was conducted on the selected mixtures. The test was performed using an Anton Paar MCR 102e rheometer equipped with a parallel-plate system comprising a fixed bottom plate and a rotating upper plate. Both plates had a sandblasted surface and a diameter of 25 mm, with a plate gap of 1 mm. Approximately 2.5 g of freshly mixed sample was loaded between the plates, after which the upper plate was lowered and any excess material was carefully trimmed. The bottom plate temperature was maintained at 20 °C using a Julabo refrigerated circulator. In the SAOS test, the storage modulus (G′) remains independent of strain only when the applied strain amplitude lies within the linear viscoelastic region (LVER). To determine the LVER of the studied mixtures, a strain sweep test was conducted at a material age of 3 min over a strain range of 0.001–50% at a constant frequency of 1 Hz. Based on the preliminary results, a strain amplitude of 0.005%, which fell within the LVER, was selected for the SAOS test. The SAOS test was then carried out at a constant frequency of 1 Hz, starting at a material age of 5 min. The test duration was 180 min, and data were recorded at 1 min intervals. Before the SAOS test, a pre-shear step of 100 s^{-1} for 30 s, followed by a 30 s resting period, was applied to ensure consistent sample conditioning. A constant normal force of 1 N was maintained on the sample to prevent wall slip during testing.

2.2.2. Low-field ^1H NMR spectroscopy

The low-field ^1H NMR measurements were performed using a Meso MR12–060V-I instrument with a magnetic field strength of 0.3 T and a resonance frequency of 12 MHz. Sample preparation followed the same procedure as that used for the isothermal calorimetry test. The ambient temperature was maintained at 20 ± 2 °C. Approximately 15 ± 0.1 g of the sample was placed into a glass vessel, which was then inserted into the sample holder. The measurement was initiated 10 min of material age, and was repeated every 10 min up to 120 min.

2.2.3. Characterization of hydration kinetics and phase assemblages

The hydration heat of studied mixtures was measured using a TAM-Air 8-channel isothermal calorimeter. All samples were prepared in a room maintained at 20 ± 2 °C. Once the instrument stabilized, 15.0 ± 0.1 g of freshly mixed sample was placed into a glass vessel and inserted into the isothermal calorimeter (the measurement was commenced 3 min after mixing for all mixtures), which was kept constantly at 20 °C. The heat flow of the sample was continuously recorded for the first 3 h. Samples were also prepared for thermogravimetric analysis (TGA) and quantitative X-ray diffraction (Q-XRD) analysis. Specimens were cured in a fog room (20 ± 2°C and >99% RH) until the designated hydration stopping times of 10 min, 1 h, and 3 h. Hydration was terminated using a solvent exchange method with isopropanol, following the procedures described by Lothenbach et al. [37]. TGA was conducted using a Netzsch STA 449 F5 Jupiter thermobalance. Approximately 10 mg of powdered sample was heated from 30 °C to 500 °C at a rate of 10 °C/min under an N_2 atmosphere with a flow rate of 20 mL/min. XRD data was acquired using a Bruker D8 Advance X-ray diffractometer with Cu-Kα radiation, operated at 40 kV and 30 mA. Diffraction data were collected over a 2θ range of 5° to 65°. To enable quantification of the amorphous phase content, 10 wt% corundum was added as an internal standard. Rietveld

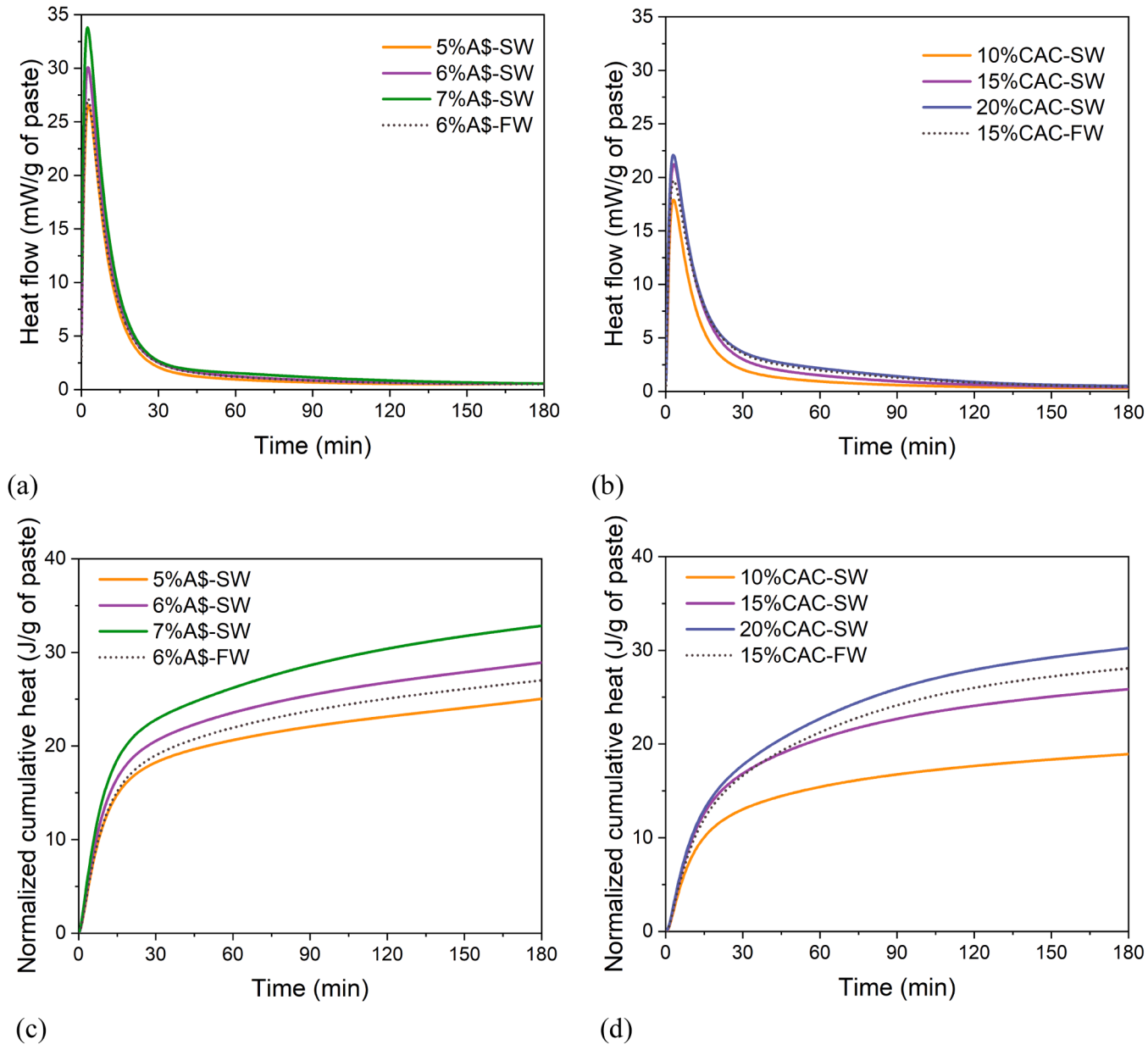


Fig. 6. Results of isothermal calorimetry test over the first 3 h: (a) Heat flow and (c) cumulative heat of cementitious material incorporating with A$-based acceleration slurry; (b) Heat flow and (d) cumulative heat of cementitious material incorporating with CAC-C$-based acceleration slurry.

refinement of all XRD patterns was performed using Profex 5.2.

3. Results

3.1. Structural build-up behaviors

Fig. 3 presents the evolution of static yield stress and the corresponding structuration rate (slope of static yield stress versus time) for the studied mixtures. For mixtures 7%A$-SW and 20%CAC-SW, the static yield stress at 75 min could not be determined due to the limited torque capacity of the rheometer. As shown in the figure, increasing the dosage of A$ or CAC-C$ accelerates the structural build-up of the fresh mixtures. Regarding the effect of seawater on static yield stress, different trends are observed for the A$ and CAC-C$ systems. In the A$ system, the use of seawater enhances the static yield stress and boosts the structuration rate throughout the first 90 min, as evidenced by the comparison between mixtures 6%A$-SW and 6%A$-FW. In contrast, for the CAC-C$ system, mixing with seawater adversely affects the structural build-up, as a slightly lower structuration rate is observed in mixture 15%CAC-SW compared to 15%CAC-FW (Fig. 3(d)). The plausible mechanisms underlying these behaviors are discussed in Sections 4.2 and 4.3.

3.2. Water states

Fig. 4 presents the T_2 relaxation time distributions of the studied mixtures at different material ages (10, 60, and 120 min). All mixtures exhibit two main peaks, located at approximately 0.01–1 ms and 1–10 ms, respectively. The first peak corresponds to water confined in interlayers, gel pores, and/or adsorbed water. The second peak is primarily attributed to water in small capillary pores. Shorter T_2 relaxation times are generally associated with smaller volumes of water [38,39]. Over time, the T_2 values of the observed peaks gradually decrease. At the beginning, this phenomenon is commonly associated with restricted water mobility within evolving particle networks. After the formation of a rigid skeleton, the decrease in the T_2 value reflects the reduction in

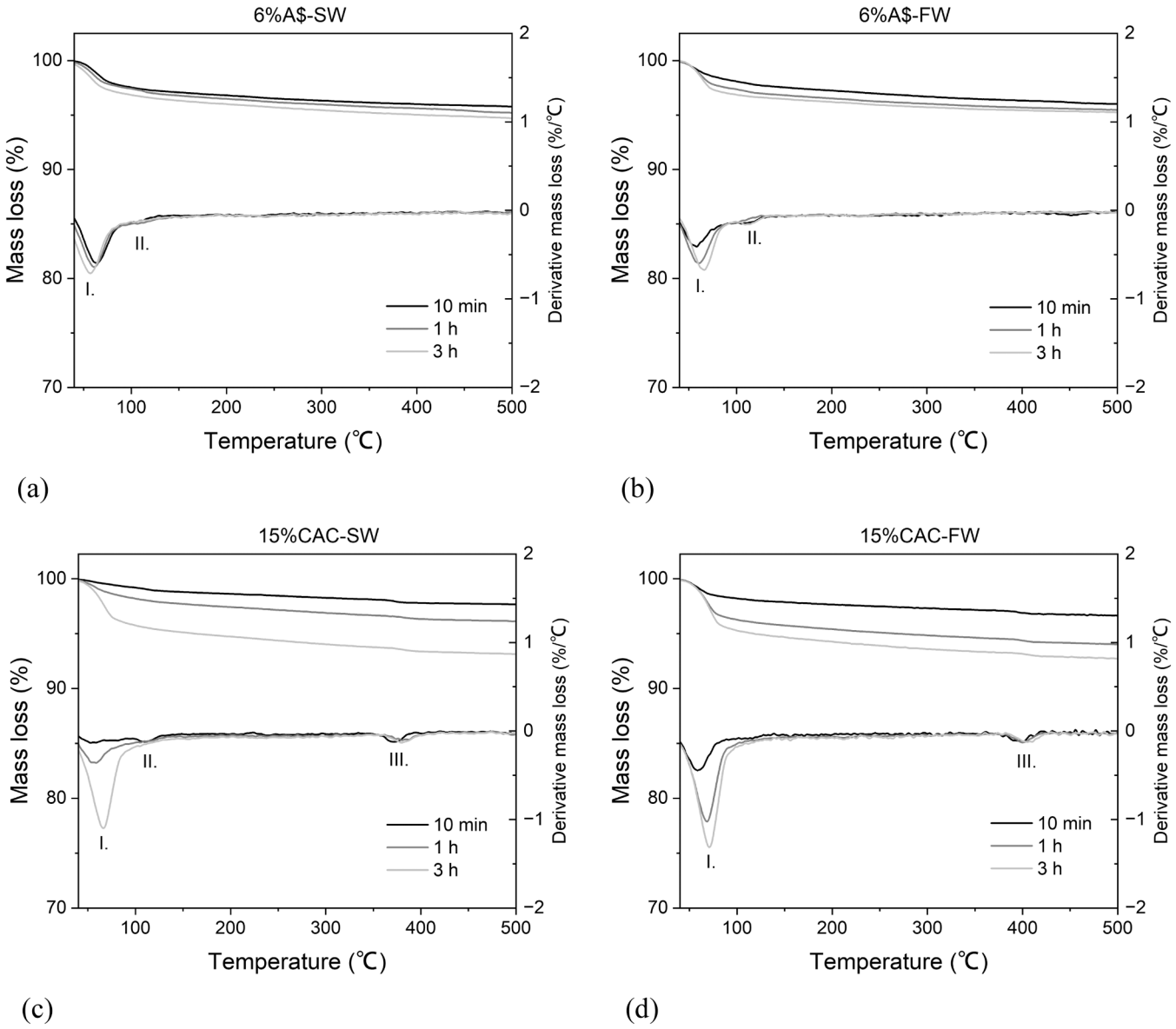


Fig. 7. TG and DTG curves at 10 min, 1 h, and 3 h: (a) Mixture 6%A$-SW; (b) Mixture 6%A$-FW; (c) Mixture 15%CAC-SW; (d) Mixture 15%CAC-FW. Peak I - C-S-H and AFt; Peak II - AFm and/or Friedel's salt; Peak III - CH.

capillary pore size as a result of physical water absorption and/or the progression of hydration processes [39–41].

To quantify the changes in the T_2 peak values, the evolution of the weighted mean T_2 value was analyzed. Surface water resulting from bleeding may appear in certain mixtures, generating signals in the range of 100–10000 ms and leading to significant fluctuations in the weighted mean T_2 value ($\overline{T_2}$). To mitigate this effect, the weighted mean T_2 was calculated within a range of 0.01–100 ms using Eq. (1).

$$\overline{T_2} = \frac{\int_{0.01}^{100} T_n I_{T_n} d\lg T_n}{\int_{0.01}^{100} I_{T_n} d\lg T_n} \quad (1)$$

where T_n is the transverse relaxation time; I_{T_n} is the corresponding relaxation intensity. Fig. 5 compares the evolution of the weighted mean T_2 value ($\overline{T_2}$) over time for different mixtures within the first 2 h. As shown in Fig. 5(a), all mixtures containing A$ exhibit similar trends, characterized by a relatively gentle slope throughout the testing period. For mixtures prepared with seawater, increasing the dosage of A$ leads to a decrease in $\overline{T_2}$. Additionally, the $\overline{T_2}$ value of mixture 6%A$-FW is slightly higher than that of 6%A$-SW, further confirming the accelerating effect of seawater ions on early-age hydration. In contrast, mixtures containing CAC-C$ display a markedly different pattern (Fig. 5(b)). All mixtures initially show higher $\overline{T_2}$ values, followed by a rapid decline within the first hour. Thereafter, the rate of decrease in $\overline{T_2}$ slows, indicating a reduced rate of microstructural development. A higher dosage of CAC-C$ leads to both a lower initial $\overline{T_2}$ value and a faster reduction rate. The presence of seawater ions results in higher values of $\overline{T_2}$ than those of the mixture prepared with fresh water at all testing times, showing a trend opposite to that observed in the A$ system. The plausible mechanisms underlying the retardation induced by seawater are summarized in Section 4.3.

The changes in water states during the first few hours can reflect the structuration process of the fresh mixture. The evolution of $\overline{T_2}$ for the studied mixtures within the first 2 h shows good agreement with the development of static yield stress (see Figs. 3 and 5). Mixtures containing A$-based acceleration slurry exhibit a relatively small $\overline{T_2}$ than those containing CAC-C$-based acceleration slurry, indicating a faster and more pronounced formation of the particle network and,

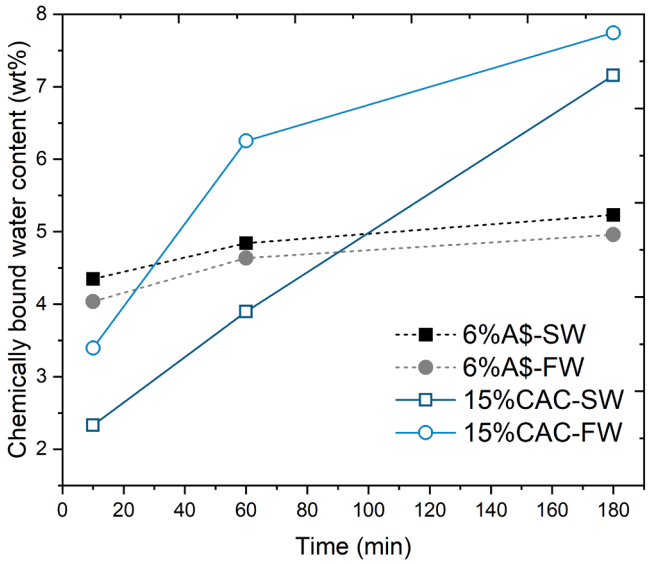


Fig. 8. TG results - the normalized amount of chemically bound water at 10 min, 1 h and 3 h.

consequently, smaller pore sizes. This interpretation is consistent with the higher heat-flow intensity of the initial peak observed in Fig. 6. After this initial stage, however, the reaction induced by A$ slows down, whereas the CAC-C$-based acceleration slurry sustains higher reactivity over a longer duration, particularly during the first 2–3 h.

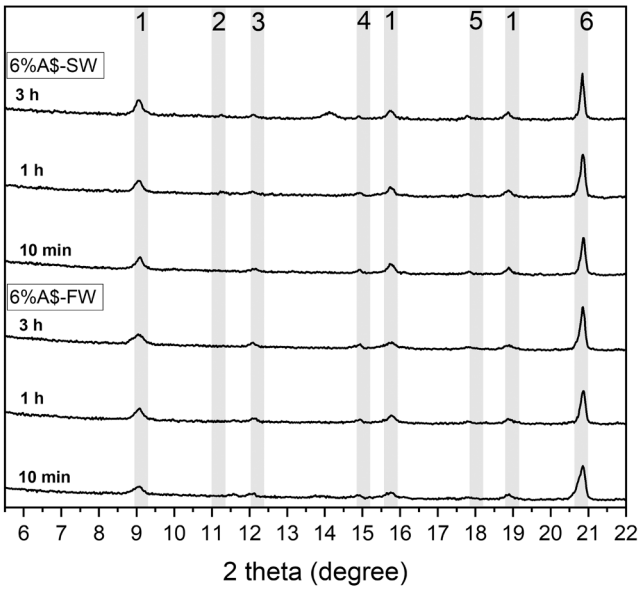
3.3. Early-age hydration

3.3.1. Hydration kinetics

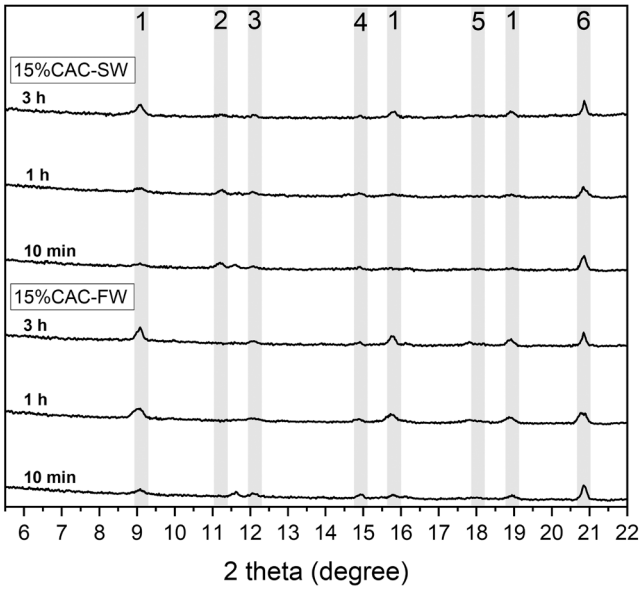
Fig. 6 illustrates the hydration kinetics of the studied mixtures during the first 3 h. For mixtures incorporating A$ slurry, an increase in A$ content leads to a higher intensity of the initial heat flow peak (Fig. 6 (a)). Replacing fresh water with seawater slightly increases the peak intensity and heat flow within the first 3 h. As shown in Fig. 6(c), a higher cumulative heat release is achieved with increasing A$ content. The use of seawater increases the cumulative heat, as evidenced by the comparison between mixtures 6%A$-SW and 6%A$-FW. For mixtures incorporating CAC-C$ slurry, a higher dosage of CAC-C$ results in a more intense initial heat flow peak (Fig. 6(b)) and a greater cumulative heat release within the first 3 h (Fig. 6(d)). Although the initial peak intensity of mixture 15%CAC-FW is slightly lower than that of 15%CAC-SW, the heat flow of 15%CAC-FW surpasses that of 15%CAC-SW after approximately 15 min of hydration. The cumulative heat of 15%CAC-FW is substantially higher than that of 15%CAC-SW, indicating that seawater exerts a negative influence on hydration heat evolution in the CAC-C$ system within the first 3 h. This behavior is consistent with the observed trends in their structural build-up. However, it should be noted that the structural build-up of fresh cementitious materials does not solely depend on hydration. Colloidal interactions between cement particles, independent of hydration, also influence the rheological properties of fresh mixtures at very early ages.

3.3.2. Phase assemblages

Fig. 7 presents the thermogravimetric (TG) and derivative thermogravimetric (DTG) curves of mixtures 6%A$-SW, 6%A$-FW, 15% CAC-SW, and 15%CAC-FW at 10 min, 1 h, and 3 h. As shown, the DTG peak observed at 100–150 °C corresponds to the dehydration of C-S-H and AFt [42]. A smaller peak between 150 and 200 °C indicates the decomposition of AFm phases and/or Friedel's salt [37]. The decomposition of calcium hydroxide (portlandite, CH) occurred in the range of 360–450 °C. Within the first 3 h, CH peaks are not noticeable in all mixtures. Thus, the quantification of CH was not conducted. The



(a)



(b)

Fig. 9. XRD results of studied mixtures at 10 min, 1 h, 3 h, 1 day and 3 days: (a) Cementitious material incorporating with A$-based acceleration slurry; (b) Cementitious material incorporating with CAC-C$-based acceleration slurry. 1- AFt, 2- Friedel's salt, 3- C_4AF, 4- C_3S, 5- CH, 6- quartz.

contents of chemically bound water were quantified using Eq. (2).

$$W_{[H_2O]} = \frac{M_{40^\circ C} - M_{500^\circ C}}{M_{500^\circ C}} \times 100(\%) \quad (2)$$

$W_{[H_2O]}$ denotes the mass fraction of chemically bound water in the mixtures. $M_{40^\circ C}$, and $M_{500^\circ C}$ mean the mass percentages at 40 °C, and 500 °C.

Fig. 8 summarizes the normalized amounts of chemically bound water in the studied mixtures at 10 min, 1 h, and 3 h. For mixtures containing CAC-C$, the use of seawater leads to decreased contents of chemically bound water, which is associated with the formation of C-S-H, CH, AFt, and Fredal's salt phases. As observed, for mixtures 6%A$-SW and 6%A$-FW, the use of seawater slightly increases the content of chemically bound water. Compared with C_3S hydration, reactions

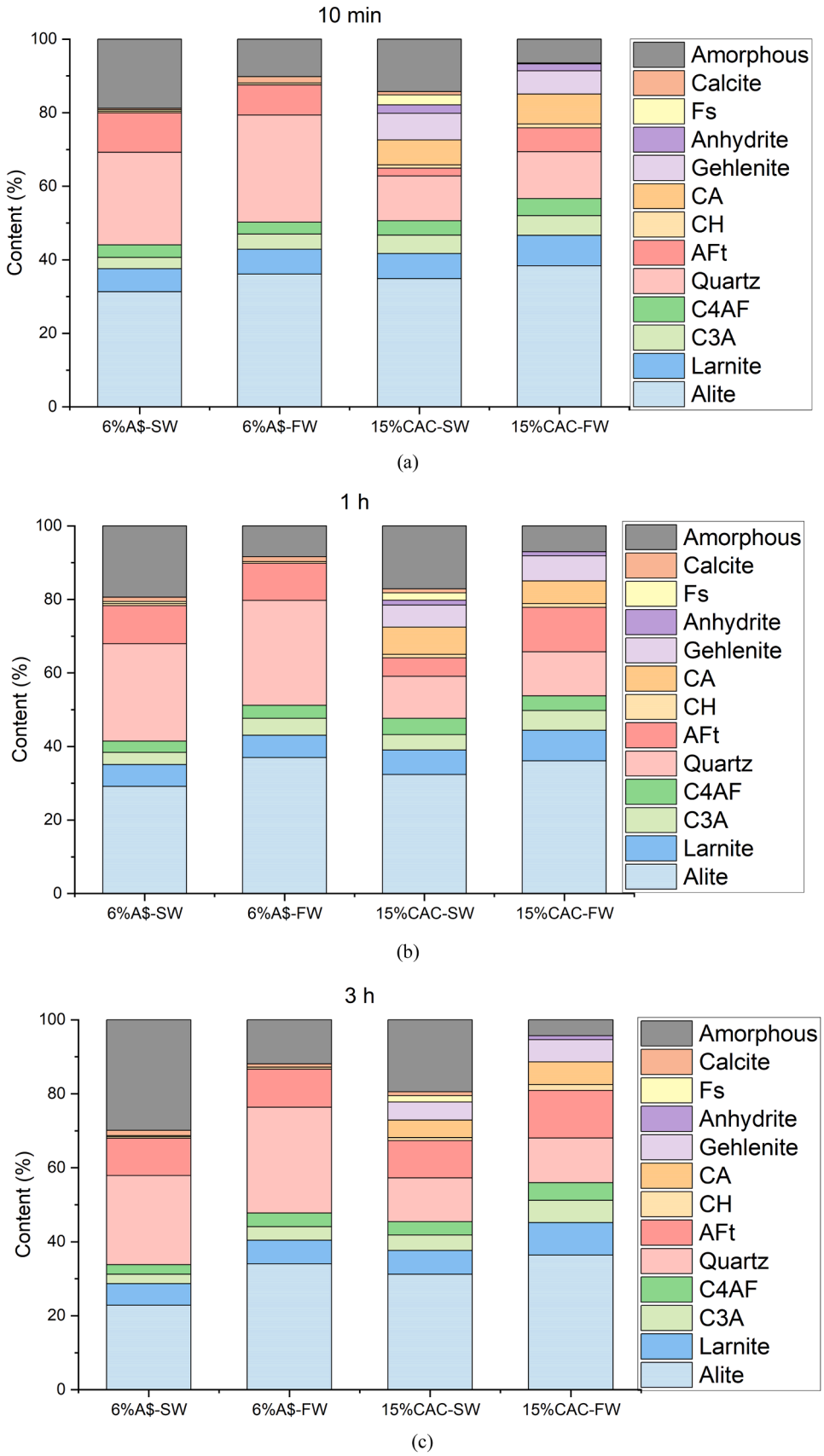


Fig. 10. Crystaline phase content of studied materials by Q-XRD at (a) 10 min, (b) 1 h, and (c) 3 h. The GOF values obtained from all refinements were below 3.5.

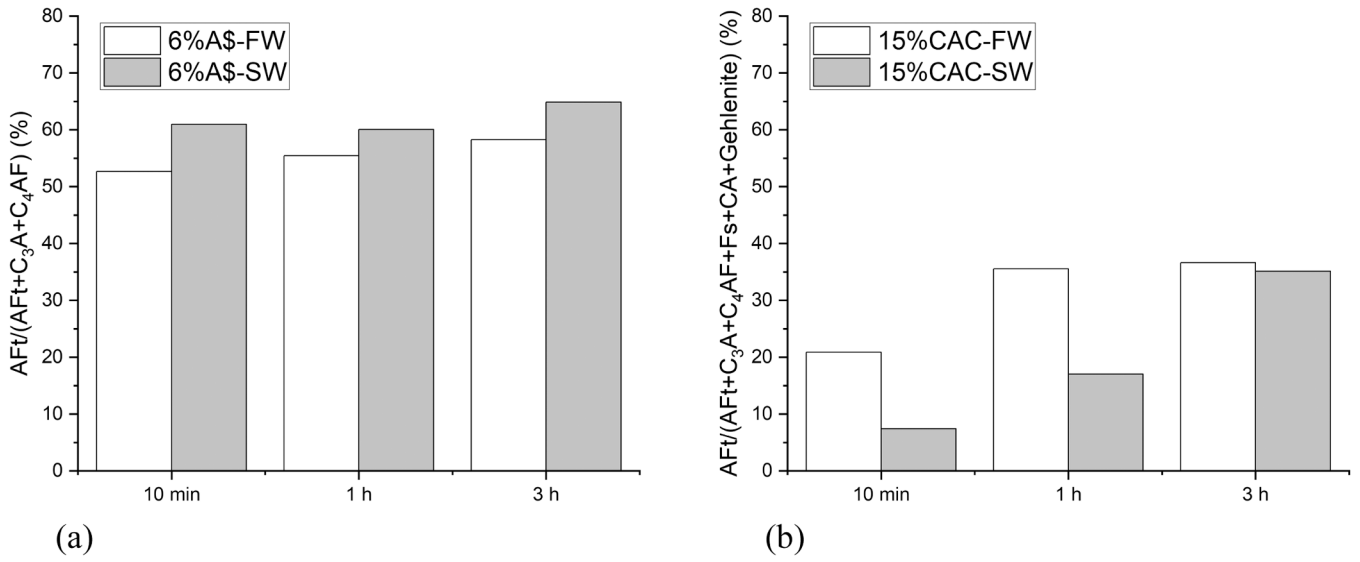


Fig. 11. AFt content relative to the amount of all phases containing aluminum: (a) Cementitious material incorporating with A$-based acceleration slurry; (b) Cementitious material incorporating with CAC-C$-based acceleration slurry. Note that the mass content of each phase was normalized by excluding the amount of chemically bound water determined from TG.

associated with AFt formation played a more dominant role in this context within the first 3 h, as further discussed in the Q-XRD analysis.

Fig. 9 reports the XRD patterns of the studied mixtures at 10 min, 1 h, and 3 h. AFt is identified as the main crystalline phase within the first 3 h for all mixtures. For the seawater-mixed systems (6%A$-SW and 15%CAC-SW), Friedel's salt is also detected. Using Rietveld refinement of the XRD data (summarized in Fig. 10), the phase assemblages of the different mixtures at 10 min, 1 h, and 3 h are determined. In both systems, mixtures prepared with seawater exhibit relatively higher contents of amorphous phases and greater C_3S consumption at each testing age, confirming the acceleration of C_3S hydration induced by seawater ions (e.g., Cl^-), as mentioned earlier. In addition, AFt is identified as the main crystalline hydration product in all studied mixtures. Mixture 15%CAC-SW exhibits a more pronounced formation of Friedel's salt compared with mixture 6%A$-SW.

The content of AFt (relative to the amount of all phases containing aluminum) for all studied mixtures is shown in Fig. 11. The formation of AFt is rapid in the mixture containing the A$-based acceleration slurry. A relatively high AFt content is observed in the A$-based system at 10 min, but the subsequent growth of AFt becomes slow. Mixture 6%A$-SW has a higher content of AFt than that of mixture 6%A$-FW. In contrast, the mixtures incorporating the CAC-C$-based acceleration slurry exhibit a relatively low AFt content at 10 min but undergo a sharp increase from 10 min to 3 h. Compared with 15%CAC-FW, 15%CAC-SW mixture shows slower AFt formation between 10 min and 1 h, indicating a retarding effect of seawater, likely associated with the concurrent formation of Friedel's salt. Overall, the evolution trends of AFt agree well with the chemically bound water content obtained from TG analysis, confirming that reactions associated with AFt formation dominate hydration within the first 3 h for all mixtures.

4. Discussion

4.1. Relationship between structural build-up and AFt formation

The evolution of static yield stress is widely regarded as a primary indicator of structural build-up in fresh cementitious materials, particularly in the context of 3DCP [13]. The measurement of static yield stress using CSR rheometry inevitably induces relative motion between particles [43]. According to Refs. [44,45], the static yield stress of fresh PC pastes at very early ages is governed by colloidal interactions, the formation of C-(A)-S-H and other early precipitates, as well as solid contacts between particles. The free water content plays a dominant role in determining the static yield stress, as it directly affects interparticle spacing and, consequently, colloidal interactions and particle contacts.

Assuming that cement particles are homogeneously suspended in the free water without segregation, the free water content determines the average interparticle distance, which controls both colloidal forces and the probability of direct particle contacts. At very early ages (e.g., 3 h in this study), C-(A)-S-H nuclei and other hydration products with relatively small volumes typically precipitate on the surfaces of cement particles [46]. Only when the interparticle distance is sufficiently reduced can adjacent particles interact through C-(A)-S-H bridges, leading to the formation of a rigid percolated network [47]. As hydration proceeds, part of the mixing water becomes physically and chemically bound, resulting in a progressive reduction in free water content. Consequently, the rate of structural build-up of fresh mixtures strongly depends on early hydration products that are capable of binding a large amount of free water at this stage, among which AFt is the most effective [12]. It should be noted that the proposed change in interparticle forces mentioned above is a hypothetical inference and was not directly measured in this study.

In this study, reactive aluminate phases (A$ and CAC-C$) were introduced into retarded seawater-mixed cementitious systems to enhance structural build-up through rapid AFt formation. As observed, the amount of AFt exhibits a strong correlation with both the static yield stress and the water state of the system (see Figs. 3 and 5). Fresh mixtures containing higher AFt contents consistently show higher static yield stresses and lower free water contents, as reflected by reduced $\overline{T_2}$ values obtained from low-field ^1H NMR measurements. Although C_3S hydration also contributes to the structural build-up of fresh cementitious materials [48], its effect is considerably less pronounced than that of AFt [12]. For example, mixture 15%CAC-SW exhibits a lower C_3S content and a higher amorphous fraction at 10 min and 1 h, yet its static yield stress is substantially lower than that of mixture 15%CAC-FW. According to Refs. [30,49], AFt can bind a substantial amount of water, up to approximately 85% relative to its mass, whereas the corresponding values for C-(A)-S-H and gypsum are only about 30%. Owing to this high bound-water content within its crystal structure, AFt develops a needle-like morphology with a large solid volume [50], which markedly increases solid contact friction between particles during static yield stress measurements.

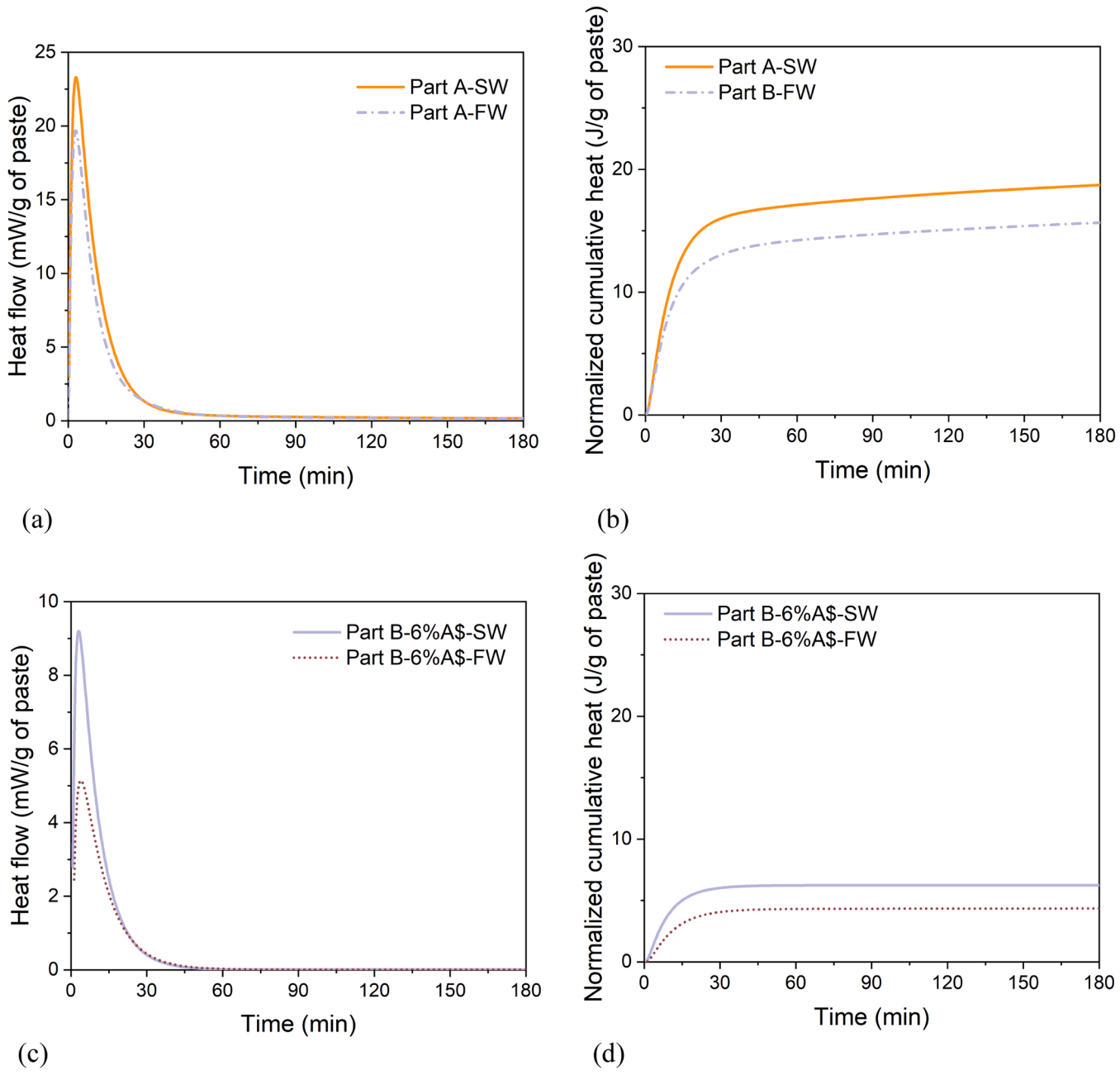


Fig. 12. Hydration kinetics of cementitious materials and acceleration slurries: (a) Heat flow and (b) cumulative heat of cementitious materials from Table 4 (Part A-SW/FW); (c) Heat flow and (d) cumulative heat of A$-based acceleration slurries from Table 4 (Part B-6%A$-SW/FW).

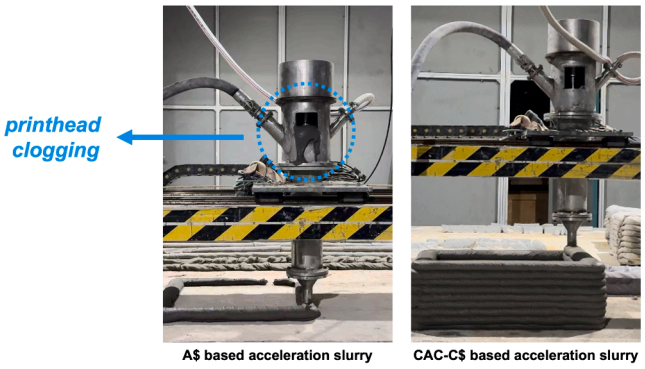
Although structural build-up in seawater-mixed cementitious systems may involve multiple concurrent mechanisms (e.g., early C-(A)-S-H formation, ionic strength effects, and Mg^{2+}-related reactions), the present results indicate that these factors play a limited role within the first 3 h. Specifically, TGA and XRD do not reveal detectable Mg-bearing hydration products, suggesting that Mg^{2+}-related reactions are not yet significant, while C_3S hydration remains minimal during this period. In contrast, a strong correlation is observed between AFt formation and the evolution of static yield stress. Therefore, early-age structuration under the investigated conditions is primarily governed by AFt precipitation, although other physicochemical effects may become relevant at later stages.

4.2. Seawater-induced enhancement of AFt formation during early hydration in the A$ system

As shown in Figs. 3 and 11, the use of seawater as mixing water enhances the early structural build-up of mixtures containing A$-based acceleration slurry within the first 3 h by promoting the rapid precipitation of AFt. Mechanistically, seawater supplies additional ionic species that facilitate AFt nucleation and growth. According to [12], AFt formation requires both an external source of Ca^{2+} and a sufficiently alkaline environment, which are provided by the pore solution of PC in the presence of A$ (see Eq. (3)).

$$2[Al(OH)_4]^- + 6Ca^{2+} + 4OH^- + 3SO_4^{2-} + 26H_2O \rightarrow 3CaO{\cdot}Al_2O_3{\cdot}3CaSO_4{\cdot}32H_2O \quad (3)$$

In the system using fresh water as the mixing water (Mixture 6%A



(a)



(b)

Fig. 13. (a) Comparison of 2 K 3D printability between the retarded seawater-mixed cementitious material using an A$-based acceleration slurry and that using a CAC-C$-based acceleration slurry (see Tables 4 and 5). Compared with mixtures 15%CAC-SW and 6%A$-SW, sand was incorporated into Part A of the printable mixtures, and the sand-to-binder ratio was maintained at 1:1. The volume ratio between Part A and Part B was about 4.8:1. The essential printing parameters were as follows: a nozzle opening diameter of 30 mm, a printing speed of 5000 mm/min, and an in-line mixing rate of 150 r/min. Part A was conveyed using a rotor-stator pump at a flow rate of 11.58 L/min, whereas Part B was delivered using a cam rotor pump at a flow rate of 2.42 L/min. (b) The printhead became blocked during the inline mixing of the retarded seawater-mixed cementitious material with the A$-based acceleration slurry. The resulting mixture adhered to the extrusion screw and exhibited extremely low free water content.

$-FW), calcium is supplied exclusively by the dissolution of clinker phases, mainly C_3S and C_3A. By contrast, when seawater is used as the mixing water (Mixture 6%A$-SW), additional calcium and sulfate ions are directly introduced via seawater (Table 3), and the early hydration of C_3S is accelerated [5,22]. As shown in Figs. 12(a) and 12(b), in cementitious systems without acceleration slurry, seawater increases both the intensity of the initial hydration peak and the cumulative heat release, indicating enhanced clinker dissolution. Therefore, seawater increases the Ca^{2+} availability in Part A, thereby promoting A$ reaction and massive AFt formation upon mixing.

Moreover, the exothermic dissolution of A$ is intensified in the presence of seawater (Figs. 12(c) and 12(d)). The Ca^{2+} ions supplied by seawater may partially react with A$ to form a limited amount of AFt within the A$ slurry prior to mixing, which likely accounts for the relatively high heat release observed. Overall, seawater ions not only facilitate AFt formation from A$ by providing a favorable chemical environment, but also enhance AFt formation in the acceleration slurry prior to its mixing with Part A.

4.3. Seawater-induced retardation of AFt formation during early hydration in the CAC-C$ system

Unlike in the A$ system, seawater delays AFt formation at early ages in the CAC-C$ system, primarily because of the delayed dissolution of C$. The seawater used in this study (Table 3) contains multiple ionic species and exhibits a high ionic strength, which can inhibit C$ dissolution through the common-ion effect [51]. The retarded dissolution of C$ limits the availability of Ca^{2+} and SO_4^{2-}, thereby suppressing the reaction between CA and sulfate to form AFt (see Eq. (4)).

$$CA + 3C\$ + (38 - x)H \rightarrow C_6A\$_3H_{32} + 2AH_3 \quad (4)$$

Although CA reacts with water to form aluminate-based hydrates, including CAH_{10}, AH_3, and C_3AH_6, the prolonged nucleation kinetics of these phases result in their persistence in an amorphous state at early ages, rendering them ineffective in promoting structural build-up in the fresh mixture [30]. Owing to the high Cl^- concentration (19042 mg/L) in seawater, Friedel's salt is preferentially and abundantly precipitated at 10 min (Fig. 10).

$$2[Al(OH)_4]^- + 4Ca^{2+} + 4OH^- + 2Cl^- + 4H_2O \rightarrow 3CaO{\cdot}Al_2O_3{\cdot}CaCl_2{\cdot}10H_2O \quad (5)$$

Compared with AFt ($C_3A{\cdot}3CaSO_4{\cdot}32\ H_2O$), Friedel's salt ($C_3A{\cdot}CaCl_2{\cdot}10\ H_2O$) binds substantially less water and exhibits a smaller solid volume, owing to its layered AFm-type structure containing limited interlayer water [52], whereas AFt possesses a columnar crystal structure with extensive water-filled channels and a significantly higher structural water content [50]. Consequently, its precipitation contributes less to early stiffness development and structural build-up of the fresh mixture than AFt.

However, the deficiency of Ca^{2+} and SO_4^{2-} appears to be confined to the very early stage. The AFt content of the 15%CAC-SW mixture at 3 h is comparable to that of the 15%CAC-FW mixture, indicating substantial AFt formation between 1 h and 3 h. In contrast, mixture 15%CAC-FW exhibits a relatively stable AFt content between 1 h and 3 h, corresponding to the extended dormant period of CAC-C$ hydration induced by SG. Notably, the retarding effect of SG appears to be partially suppressed in the presence of seawater. This behavior may be attributed to interactions between seawater ions and SG, which warrant further investigation.

Additionally, in this study, we attributed the observed structural build-up behavior of the studied mixtures to multiple mechanisms, including ion availability, nucleation density, and crystal morphology; however, their individual effects cannot be conclusively separated based on the current results. A more comprehensive investigation into the contribution of each mechanism should be the focus of future work.

4.4. Comparison between A$ and CAC-C$ as acceleration slurry in seawater-mixed concrete 2 K 3D printing

As an acceleration slurry for retarded seawater-mixed cementitious materials in 2 K 3DCP, CAC-C$ outperforms A$ in terms of tunability and sustained buildability support. Accordingly, mixtures 6%A$-SW and 15%CAC-SW were selected for comparison, as they exhibit similar static yield stress within the first 30 min and 28-day compressive strengths (~52 MPa). As shown in Fig. 14(a), mixture 15%CAC-SW presents a slightly lower static yield stress than 6%A$-SW at 10 min, which is attributed to the rapid initial reaction of A$ (Section 4.2). However, the extensive AFt precipitation induced by A$ rapidly consumes free water, leading to reduced cohesion and severe printhead clogging during the 2 K 3DCP process (Fig. 13). In contrast, the CAC-C$-based acceleration slurry enables a more controlled AFt formation rate, resulting in a lower yield stress during inline mixing and thus a more stable printability window. It should be noted that the printability of these mixtures was evaluated based on rheological trends and visual observations.

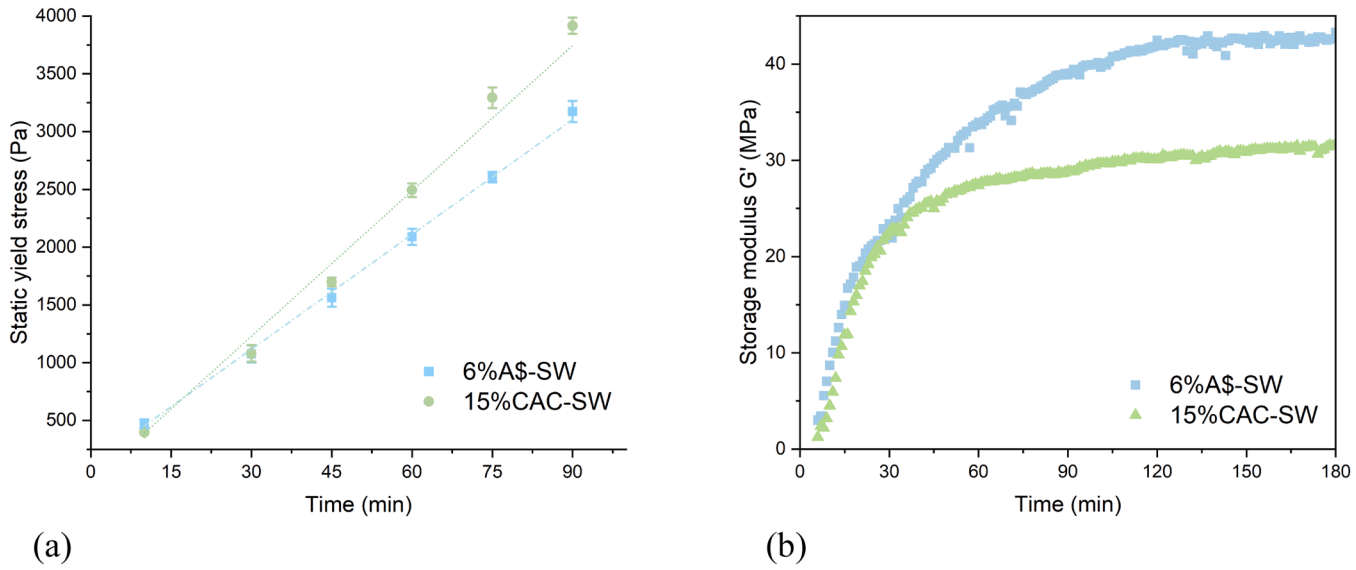


Fig. 14. Comparison of (a) structural build-up and (b) elasticity evolution between mixtures 15%CAC-SW and 6%A$-SW.

Table 6
Alite and amorphous phase contents (wt%) determined by Q-XRD. The mass content of each phase was normalized by excluding the chemically bound water acquired from TG.

	6%A$-SW		15%CAC-SW	
Time	Alite	Amorphous phase	Alite	Amorphous phase
10 min	24.59	14.76	27.38	11.23
1 h	23.03	15.33	25.60	13.58
3 h	18.09	23.71	24.74	15.46

After 30 min, mixture 15%CAC-SW develops a higher static yield stress than 6%A$-SW, providing enhanced structural support for buildability. Time-sweep rheological tests conducted within the first 180 min reveal that mixture 6%A$-SW exhibits a higher storage modulus (G′), indicating accelerated C-(A)-S-H nucleation (Fig. 14(b)). This is corroborated by Q-XRD results (Table 6), which show greater C_3S consumption and increased amorphous phase formation in 6%A$-SW. Nevertheless, as discussed in Section 4.1, early-stage C-(A)-S-H nucleation contributes less effectively to static yield stress development than AFt formation. This is consistent with Roussel et al. [44], who noted that a high G′ does not necessarily correspond to a high static yield stress due to differences in testing mechanisms.

4.5. Limitations of the current study

It should be acknowledged that most of the tests in this study do not include validation through full-scale 2 K printing, and instead adopts a simplified laboratory mixing approach for combining Parts A and B. This choice was made intentionally, as the primary objective is to elucidate the fundamental interactions among seawater ions, Portland cement, and aluminate-based accelerators (including A$ and CAC-C$), rather than to optimize a practical 2 K printing process. The simplified mixing strategy provides better control of experimental variables and helps avoid additional process-induced complexities associated with inline mixing, such as spatial inhomogeneity, fluctuating flow conditions, and time-dependent mixing efficiency, which could obscure the intrinsic physicochemical mechanisms governing early-age hydration and structural build-up.

However, this simplification also introduces a limitation in terms of direct applicability to real 2 K printing systems. The rheological parameters used in this study (e.g., static yield stress and storage modulus) serve as indicators of structural build-up and buildability, but they cannot fully capture deposition-related behaviors such as filament stability, interlayer bonding, and real-time mixing uniformity. Therefore, caution should be exercised when extrapolating the present findings to practical printing conditions. Nevertheless, the results provide meaningful mechanistic insights into seawater–cement–accelerator interactions, and future work will focus on validating and extending these findings through full-scale 2 K printing under realistic operational conditions.

Additionally, the relationships among the results obtained from different characterization techniques are interpreted primarily in a qualitative manner. Although establishing quantitative correlations would provide deeper insight into early-age structuration, this remains challenging due to differences in measurement principles and temporal resolution. In particular, the effective measurement windows are not fully aligned. For example, static yield stress could only be reliably determined within the first 60–90 min due to rheometer torque limitations, whereas other techniques extend over longer timescales. As a result, the discussion focuses on the consistency of trends and temporal correspondence across independent measurements rather than strict one-to-one correlations.

5. Conclusion

In this work, we proposed the use of aluminate-based acceleration slurries to “wake up” retarded seawater-mixed cementitious materials by controlling AFt formation, thereby achieving the desired set-on-demand performance in the context of 2 K 3DCP. Two types of acceleration slurries, based on A$ and CAC-C$, were employed and systematically compared in terms of their effects on structural build-up, early-age hydration, and phase assemblage evolution. In addition, the interactions among seawater ions, PC, and aluminate-based acceleration slurries, particularly their impact on AFt formation, were comprehensively discussed. The main findings of this study are summarized as follows:

- Both A$- and CAC-C$-based acceleration slurries effectively enhance the structural build-up of retarded seawater-mixed cementitious materials. Increasing the dosage of either A$ or CAC-C$ further accelerates the evolution of structuration.
- In both acceleration systems, AFt formation governs the structural build-up of seawater-mixed materials. Owing to its high free-water

binding capacity and voluminous needle-like morphology, AFt significantly enhances interparticle contacts and contributes more effectively to static yield stress development than C_3S hydration alone during the first 3 h.

- Seawater significantly enhances the early structural build-up of the A$-based system by promoting rapid AFt formation through increased availability of Ca^{2+} and sulfate ions and accelerated clinker dissolution. By establishing a chemically favorable environment, seawater not only intensifies AFt precipitation within the cementitious matrix but also facilitates pre-reaction in the acceleration slurry, thereby strengthening early hydration kinetics.
- In contrast, seawater initially suppresses AFt formation in the CAC-C$ system by retarding C$ dissolution and promoting the preferential precipitation of Friedel's salt, which binds less water and contributes less to structural build-up. Nevertheless, this inhibitory effect is transient, as AFt formation recovers at later ages.
- Although the A$-based system promotes rapid early stiffening, excessive AFt formation compromises process stability and leads to printhead clogging during 2 K 3DCP. In comparison, the CAC-C$-based acceleration slurry provides greater tunability, ensures a stable printability window, and delivers sustained structural build-up at later times, demonstrating superior overall performance for practical seawater-mixed concrete 3D printing applications.

CRediT authorship contribution statement

Yamei Zhang: Supervision, Resources, Project administration, Funding acquisition, Conceptualization. **Yilin Zhao:** Software, Investigation. **Xusheng Chen:** Software, Investigation. **Yu Zeng:** Writing – review & editing, Validation, Methodology, Formal analysis. **Zhipeng Li:** Software, Investigation. **Yiqun Xue:** Visualization, Validation, Software, Investigation. **Yao Li:** Visualization, Validation, Investigation, Formal analysis, Data curation. **Yu Chen:** Writing – review & editing, Writing – original draft, Supervision, Project administration, Methodology, Funding acquisition, Formal analysis, Conceptualization.

Declaration of Competing Interest

The authors declare that they have no known competing financial interests or personal relationships that could have appeared to influence the work reported in this paper.

Acknowledgement

The authors would like to acknowledge the funding supported by National Natural Science Foundation of China (NSFC) (Grant No. 52402021), Natural Science Foundation of Jiangsu Province (Grant No. BK20241338), the Start-up Research Fund of Southeast University (Grant No. RF1028624009).

Appendix

Table A1
The ionic composition of the Yellow Sea seawater determined using ICP-MS and IC

Ions	Cl^-	Na^+	SO_4^{2-}	Mg^{2+}	Ca^{2+}	K^+	Others	pH
Seawater (mg/L)	19042	10864	2687	1221	523	320	160	7.9

Data availability

Data will be made available on request.

References

[1] U. Ebead, D. Lau, F. Lollini, A. Nanni, P. Suraneni, T. Yu, A review of recent advances in the science and technology of seawater-mixed concrete, Cem. Concr. Res. 152 (2022) 106666, https://doi.org/10.1016/j.cemconres.2021.106666.
[2] Y. Cai, Y. Tao, D. Xuan, X. Zhu, C.S. Poon, Effects of seawater on the formation and mechanical properties of Friedel's salt associated with tricalcium aluminate, Cem. Concr. Res. 174 (2023) 107340, https://doi.org/10.1016/j.cemconres.2023.107340.
[3] K. Zhang, Q. Zhang, J. Xiao, Durability of FRP bars and FRP bar reinforced seawater sea sand concrete structures in marine environments, Constr. Build. Mater. 350 (2022) 128898, https://doi.org/10.1016/j.conbuildmat.2022.128898.
[4] P. Li, W. Li, Z. Sun, L. Shen, D. Sheng, Development of sustainable concrete incorporating seawater: a critical review on cement hydration, microstructure and mechanical strength, Cem. Concr. Compos. 121 (2021) 104100, https://doi.org/10.1016/j.cemconcomp.2021.104100.
[5] P. Li, W. Li, T. Yu, F. Qu, V.W.Y. Tam, Investigation on early-age hydration, mechanical properties and microstructure of seawater sea sand cement mortar, Constr. Build. Mater. 249 (2020) 118776, https://doi.org/10.1016/j.conbuildmat.2020.118776.
[6] J. Wang, J. Xie, Y. Wang, Y. Liu, Y. Ding, Rheological properties, compressive strength, hydration products and microstructure of seawater-mixed cement pastes, Cem. Concr. Compos. 114 (2020) 103770, https://doi.org/10.1016/j.cemconcomp.2020.103770.
[7] R.A. Buswell, W.R. Leal de Silva, S.Z. Jones, J. Dirrenberger, 3D printing using concrete extrusion: a roadmap for research, Cem. Concr. Res. 112 (2018) 37–49, https://doi.org/10.1016/j.cemconres.2018.05.006.
[8] G. De Schutter, K. Lesage, V. Mechtcherine, V.N. Nerella, G. Habert, I. Agusti-Juan, Vision of 3D printing with concrete — Technical, economic and environmental potentials, Cem. Concr. Res. 112 (2018) 25–36, https://doi.org/10.1016/j.cemconres.2018.06.001.
[9] S.H. Chu, L.G. Li, A.K.H. Kwan, Development of extrudable high strength fiber reinforced concrete incorporating nano calcium carbonate, Addit. Manuf. 37 (2021) 101617, https://doi.org/10.1016/j.addma.2020.101617.
[10] M. Chen, H. Li, L. Yang, S. Wang, P. Zhao, Y. Huang, L. Lu, G. Yue, Q. Li, Rheology and shape stability control of 3D printed calcium sulphoaluminate cement composites containing paper milling sludge, Addit. Manuf. 54 (2022) 102781, https://doi.org/10.1016/j.addma.2022.102781.
[11] L. Wang, Y. Liu, Y. Yang, Y. Li, M. Bai, Bonding performance of 3D printing concrete with self-locking interfaces exposed to compression–shear and compression–splitting stresses, Addit. Manuf. 42 (2021) 101992, https://doi.org/10.1016/j.addma.2021.101992.
[12] T. Wangler, Y. Tao, A. Das, M. Mahmoudi, S. Gürel, R.J. Flatt, Aluminate 2K systems in digital concrete: process, design, chemistry, and outlook, Cem. Concr. Res. 185 (2024) 107644, https://doi.org/10.1016/j.cemconres.2024.107644.
[13] N. Roussel, Rheological requirements for printable concretes, Cem. Concr. Res. 112 (2018) 76–85, https://doi.org/10.1016/j.cemconres.2018.04.005.
[14] L. Reiter, T. Wangler, N. Roussel, R.J. Flatt, The role of early age structural build-up in digital fabrication with concrete, Cem. Concr. Res. 112 (2018) 86–95, https://doi.org/10.1016/j.cemconres.2018.05.011.
[15] D. Marchon, S. Kawashima, H. Bessaies-Bey, S. Mantellato, S. Ng, Hydration and rheology control of concrete for digital fabrication: potential admixtures and cement chemistry, Cem. Concr. Res. 112 (2018) 96–110, https://doi.org/10.1016/j.cemconres.2018.05.014.
[16] T. Wangler, R. Pileggi, S. Gürel, R.J. Flatt, A chemical process engineering look at digital concrete processes: critical step design, inline mixing, and scaleup, Cem. Concr. Res. 155 (2022) 106782, https://doi.org/10.1016/j.cemconres.2022.106782.
[17] Y. Chen, S. Chaves Figueiredo, Z. Li, Z. Chang, K. Jansen, O. Çopuroğlu, E. Schlangen, Improving printability of limestone-calcined clay-based cementitious materials by using viscosity-modifying admixture, Cem. Concr. Res. 132 (2020) 106040, https://doi.org/10.1016/j.cemconres.2020.106040.
[18] V.N. Nerella, M. Näther, A. Iqbal, M. Butler, V. Mechtcherine, Inline quantification of extrudability of cementitious materials for digital construction, Cem. Concr.

Compos. 95 (2019) 260–270, https://doi.org/10.1016/j.cemconcomp.2018.09.015.
[19] S. Kawashima, K. Wang, R.D. Ferron, J.H. Kim, N. Tregger, S. Shah, A review of the effect of nanoclays on the fresh and hardened properties of cement-based materials, Cem. Concr. Res. 147 (2021) 106502, https://doi.org/10.1016/j.cemconres.2021.106502.
[20] L. Reiter, T. Wangler, N. Roussel, R.J. Flatt, The role of early age structural build-up in digital fabrication with concrete, Cem. Concr. Res. 112 (2018) 86–95, https://doi.org/10.1016/j.cemconres.2018.05.011.
[21] Y. Chen, S. He, Y. Zhang, Z. Wan, O. Çopuroğlu, E. Schlangen, 3D printing of calcined clay-limestone-based cementitious materials, Cem. Concr. Res. 149 (2021) 106553, https://doi.org/10.1016/j.cemconres.2021.106553.
[22] Y. Chen, N. Toosumran, N. Chehab, H. Spanjers, O. Çopuroğlu, Feasibility study of using desalination brine to control the stiffness and early-age hydration of 3D printable cementitious materials, J. Clean. Prod. 378 (2022) 134522, https://doi.org/10.1016/j.jclepro.2022.134522.
[23] A. Anton, L. Reiter, T. Wangler, V. Frangez, R.J. Flatt, B. Dillenburger, A 3D concrete printing prefabrication platform for bespoke columns, Autom. Constr. 122 (2021) 103467, https://doi.org/10.1016/j.autcon.2020.103467.
[24] F. Boscaro, E. Quadranti, T. Wangler, S. Mantellato, L. Reiter, R.J. Flatt, Eco-Friendly, Set-on-Demand Digital Concrete, D Print. Addit. Manuf. (2021) 3, https://doi.org/10.1089/3dp.2020.0350.
[25] V. Mechtcherine, F.P. Bos, A. Perrot, W.R.R.L. da Silva, V.N. Nerella, S. Fataei, R.J. M. Wolfs, M. Sonebi, N. Roussel, Extrusion-based additive manufacturing with cement-based materials – production steps, processes, and their underlying physics: a review, Cem. Concr. Res. 132 (2020) 106037, https://doi.org/10.1016/j.cemconres.2020.106037.
[26] Y. Tao, A.V. Rahul, K. Lesage, Y. Yuan, K. Van Tittelboom, G. De Schutter, Stiffening control of cement-based materials using accelerators in inline mixing processes: possibilities and challenges, Cem. Concr. Compos. 119 (2021) 103972, https://doi.org/10.1016/j.cemconcomp.2021.103972.
[27] C. Gosselin, R. Duballet, P. Roux, N. Gaudillière, J. Dirrenberger, P. Morel, Large-scale 3D printing of ultra-high performance concrete - a new processing route for architects and builders, Mater. Des. 100 (2016) 102–109, https://doi.org/10.1016/j.matdes.2016.03.097.
[28] Y. Chen, H. Rahmani, E. Schlangen, O. Çopuroğlu, An approach to develop set-on-demand 3D printable limestone-calcined clay-based cementitious materials using calcium nitrate, Cem. Concr. Compos. 145 (2024) 105373, https://doi.org/10.1016/j.cemconcomp.2023.105373.
[29] L. Reiter, T. Wangler, A. Anton, R.J. Flatt, Setting on demand for digital concrete – Principles, measurements, chemistry, validation, Cem. Concr. Res. 132 (2020) 106047, https://doi.org/10.1016/j.cemconres.2020.106047.
[30] A. Das, L. Reiter, S. Mantellato, R.J. Flatt, Early-age rheology and hydration control of ternary binders for 3D printing applications, Cem. Concr. Res. 162 (2022) 107004, https://doi.org/10.1016/j.cemconres.2022.107004.
[31] A. Quennoz, K.L. Scrivener, Interactions between alite and C3A-gypsum hydrations in model cements, Cem. Concr. Res. 44 (2013) 46–54, https://doi.org/10.1016/j.cemconres.2012.10.018.
[32] S.T. Bergold, F. Goetz-Neunhoeffer, J. Neubauer, Interaction of silicate and aluminate reaction in a synthetic cement system: implications for the process of alite hydration, Cem. Concr. Res. 93 (2017) 32–44, https://doi.org/10.1016/j.cemconres.2016.12.006.
[33] Y. Cai, D. Xuan, P. Hou, J. Shi, C.S. Poon, Effect of seawater as mixing water on the hydration behaviour of tricalcium aluminate, Cem. Concr. Res. 149 (2021) 106565, https://doi.org/10.1016/j.cemconres.2021.106565.
[34] A. Das, C. Wenger, L. Walpen, R.J. Flatt, Early-age hydration of accelerated low-carbon cements for digital fabrication, Cem. Concr. Compos. 159 (2025) 105991, https://doi.org/10.1016/j.cemconcomp.2025.105991.
[35] Y. Tao, M.K. Mohan, A.V. Rahul, G. De Schutter, K. Van Tittelboom, Development of a calcium sulfoaluminate-Portland cement binary system for twin-pipe 3D concrete printing, Cem. Concr. Compos. 138 (2023) 104960, https://doi.org/10.1016/j.cemconcomp.2023.104960.
[36] Y. Tao, M.K. Mohan, A.V. Rahul, Y. Yuan, G. De Schutter, K. Van Tittelboom, Stiffening controllable concrete modified with redispersible polymer powder for twin-pipe printing, Cem. Concr. Res. 161 (2022) 106953, https://doi.org/10.1016/j.cemconres.2022.106953.
[37] B. Lothenbach, P. Durdzinski, K.De Weerdt, Thermogravimetric analysis, in: K. Scrivener, R. Snellings, B. Lothenbach (Eds.), A Pract. Guid. to Microstruct. Anal. Cem. Mater, CRC press, 2016, pp. 177–212.
[38] T. Huang, Q. Yuan, S. Zuo, Y. Xie, C. Shi, New insights into the effect of gypsum on hydration and elasticity development of C3S paste during setting, Cem. Concr. Res. 159 (2022) 106860, https://doi.org/10.1016/j.cemconres.2022.106860.
[39] H. Liu, Z. Sun, J. Yang, Y. Ji, A novel method for semi-quantitative analysis of hydration degree of cement by 1H low-field NMR, Cem. Concr. Res. 141 (2021) 106329, https://doi.org/10.1016/j.cemconres.2020.106329.
[40] M.W. Bligh, M.N. D'Eurydice, R.R. Lloyd, C.H. Arns, T.D. Waite, Investigation of early hydration dynamics and microstructural development in ordinary Portland cement using ^{1}H NMR relaxometry and isothermal calorimetry, Cem. Concr. Res. 83 (2016) 131–139, https://doi.org/10.1016/j.cemconres.2016.01.007.
[41] Y. Ji, Z. Sun, X. Yang, C. Li, X. Tang, Assessment and mechanism study of bleeding process in cement paste by 1H low-field NMR, Constr. Build. Mater. 100 (2015) 255–261, https://doi.org/10.1016/j.conbuildmat.2015.09.062.
[42] K. De Weerdt, M.Ben Haha, G. Le Saout, K.O. Kjellsen, H. Justnes, B. Lothenbach, Hydration mechanisms of ternary Portland cements containing limestone powder and fly ash, Cem. Concr. Res. 41 (2011) 279–291, https://doi.org/10.1016/j.cemconres.2010.11.014.
[43] Y. Chen, O. Çopuroğlu, Understanding the role of calcined clay in yield stress evolution of LC3 with ultra-high volume of calcined clay and limestone, Constr. Build. Mater. 492 (2025) 142898, https://doi.org/10.1016/j.conbuildmat.2025.142898.
[44] N. Roussel, H. Bessaies-Bey, S. Kawashima, D. Marchon, K. Vasilic, R. Wolfs, Recent advances on yield stress and elasticity of fresh cement-based materials, Cem. Concr. Res. 124 (2019) 105798, https://doi.org/10.1016/j.cemconres.2019.105798.
[45] Y. Qian, S. Kawashima, Distinguishing dynamic and static yield stress of fresh cement mortars through thixotropy, Cem. Concr. Compos. 86 (2018) 288–296, https://doi.org/10.1016/j.cemconcomp.2017.11.019.
[46] K.L. Scrivener, P. Juilland, P.J.M. Monteiro, Advances in understanding hydration of Portland cement, Cem. Concr. Res. 78 (2015) 38–56, https://doi.org/10.1016/j.cemconres.2015.05.025.
[47] N. Roussel, A. Lemaître, R.J. Flatt, P. Coussot, Steady state flow of cement suspensions: a micromechanical state of the art, Cem. Concr. Res. 40 (2010) 77–84, https://doi.org/10.1016/j.cemconres.2009.08.026.
[48] S.Z. Jones, J.B. Hipp, A.J. Allen, C.V. Gagnon, Rheology and microstructure development of hydrating tricalcium silicate - implications for additive manufacturing in construction, Cem. Concr. Res. 152 (2022) 106651, https://doi.org/10.1016/j.cemconres.2021.106651.
[49] J.H. Ideker, K.L. Scrivener, H. Fryda, B. Touzo. Calcium Aluminate Cements, Fourth Edi, Elsevier Ltd, 2019, https://doi.org/10.1016/B978-0-08-100773-0.00012-5.
[50] F. Goetz-Neunhoeffer, J. Neubauer, Refined ettringite (Ca 6 Al 2 (SO 4) 3 (OH) 12 •26H 2 O) structure for quantitative X-ray diffraction analysis, Powder Diffr. 21 (2006) 4–11, https://doi.org/10.1154/1.2146207.
[51] Z. Li, G.P. Demopoulos, Solubility of CaSO4 phases in aqueous HCl + CaCl2 solutions from 283 K to 353 K, J. Chem. Eng. Data 50 (2005) 1971–1982, https://doi.org/10.1021/je050217e.
[52] H.F.W. Taylor. Cement Chemistry, 2nd ed., Emerald Publishing Limited, 1997 https://doi.org/10.1680/cc.25929.